Akademie věd České republiky

Teze disertace
k získání vědeckého titulu "doktor věd"
ve skupině věd FYZIKÁLNĚ-MATEMATICKÉ VĚDY

ELECTRONIC STRUCTURE THEORY OF COMPLEX ACTINIDE MATERIALS WITH STRONG COULOMB INTERACTIONS.

Komise pro obhajoby doktorských disertací v oboru fyzika kondenzovaných systémů

Jméno uchazeče: Ing., Alexander B. Shick, CSc

Pracoviště uchazeče: Fyzikální ústav Akademie věd České republiky, v. v. i.

Misto a datum: Praha, květen 2014

Preface: The results of this thesis are obtained in collaboration and intense scientific interaction with the colleagues from the Department of Condensed Matter theory. I take an opportunity to thank V. Janiš, J. Kolorenč, V. Drchal, as well as A. I. Lichtenstein (University of Hamburg), J. Rusz and P. Oppeneer (Uppsala University). Also, I would like to thank W. E. Pickett (UC Davis) for his involvement at earlier stages of this work, and P. Novak and J. Kuneš for helpful discussions. The work on actinides is closely tied to experimental developments, and I thank L. Havela from the Department of Condensed Matter Physics, Charles University, Prague, T. Klimczuk, Th. Gouder, R. Eloirdi, and R. Caciuffo from the European Commission Institute for Transuranium Elements (ITU - Karlsruhe) for sharing and intensly discussing with me their experimental results.

Contents

1 Introduction

The aim of this work is to understand the physical phenomena in actinide based materials. In order to realize the full potential of nuclear power, and to avoid the risks for society and environment, there is a need to solve many problems in the material science of actinides, by advancing the comprehension of their physical and chemical properties at the nanoscale level. This study can assist to form a basis for realistic modeling of the materials used for the nuclear energy production, and save and secure disposal of the nuclear waste.

Theoretical modeling of the electronic, structural, and magnetic character of actinide materials and their 5f-manifold states is very difficult. The standard electronic structure tools of solid state physics based on the density functional theory (DFT) cannot be taken as a reliable vehicle to explain the electronic, structural and magnetic properties of heavy actinides and their compounds. The unique physical properties of actinides originate of their position at the localization-delocalization threshold, and require new many body tools and concepts.

In this thesis, I summarize the effort to provide the material-specific theory based on combination of the relativistic DFT including the spin-orbit coupling with the rotationally invariant multi-orbital Coulomb interaction. I will focus on the actinide based materials where the relativistic effects play a very essential role for the band structure and interaction components of the model. I will describe the correlated band theory methods: (i) static local (spin) density plus Coulomb U (LDA+U) and (ii) dynamical LDA+Hubbard-I (LDA+HIA) and LDA+Exact Diagonalization (LDA+ED) approximations implemented in the full-potential linearized augmented plane wave basis (FP-LAPW).

This thesis is based on the papers collected in the "List of papers", which are listed in a chronological order, and are reffered to in the text by their Roman numerals. The thesis is organized as follows:

- In Chapter II. I describe the methods of the modern correlated electron theory of solid state with emphasis on original developments in a fields of the static and dynamical mean-field theories, and their implementation in the FP-LAPW basis. Specific attention is given to the relativistic interactions - mostly spin-orbit coupling - within a framework of LDA+U method. This section is based on papers **I, II, III, V**.

  The examples of LDA+U application to selected U and Np inter metallic compounds are given. It is shown that LDA+U produces the orbital polarization which helps to explain orbital magnetic moments and the magnetic anisotropy in selected nanostructures and f-electron materials. This section is based on papers **III, IV, XI, XIII, XIV**.

  Next, the extension of LDA+U to include the multi-determinant configurational interaction effects is given. It is based on the combination of the LDA with the many-body solution of the Anderson impurity model, and follows the dynamical mean-field theory (DMFT). The dynamical LDA+Hubbard-I (LDA+HIA) and LDA+"Exact Diagonalization" (LDA+ED) approximations are formulated together with the self-consistent charge density calculations. This section is based on papers **VI-VIII, XII, XV**.

  As an example, the applications of LDA+HIA to the electronic structure and photoemission of the elemental Am and Cm are given. It is shown that multiplet transitions need to be incorporated into the electronic structure calculations in order to reproduce experimental data. This section is based on papers **VIII,IX**.

- In Chapter III. I discuss the electronic and magnetic properties of of δ-Pu. it is shown that *around-mean-field* LDA+U is capable to explain the non-magnetic character of δ-Pu ground state. The application of LDA+HIA and LDA+ED allows to incorporate the multiplet transitions into the electronic structure calculations, and to explain the photoemission spectroscopy data. It is shown that the singlet ground state can form in δ-Pu, with the local 5f magnetic moment is compensated by a moment in the surrounding cloud of conduction electrons. This chapter is based on papers **VI, VIII, XV**.

- Chapter IV. desribes the most recent results of the electronic structure and superconductivity in $PuCoGa_5$ and related family of materials (often called Pu115), a compound exhibiting superconductivity below a critical temperature that is one order of magnitude higher than for typical heavy-fermion compounds. he electron-pairing mechanism in the Pu-115 family is still obscure, and is the subject of heated debates.

  I address the electron correlation effects in the Pu-115 family, in comparison with elemental plutonium. It is shown that the singlet ground state can form in PuCoGa5 similar to δ-Pu, with the local 5f magnetic moment is compensated by a moment in the surrounding cloud of conduction electrons. On the basis of these results, the nature of the unconventional d-wave superconducting state in PuCoIn5 and PuCoGa5 is discussed. It is suggested that fluctuations of the residual magnetic moment as well as as valence fluctuations are a key ingredient of superconductivity in these compounds. This chapter is based on papers **V, X, XII, XV**.

2 Methods of correlated band theory

Density-functional theory (DFT) and its associated local (spin) density approximation (LSDA), and generalized gradient approximation (GGA) are used, often with great success, to describe the properties of a wide variety of materials. However there exists a class of materials which are poorly described by LSDA/GGA. These so-called strongly correlated materials typically contain atoms with open f shells, in which the corresponding orbitals are localized.

In the past two decades several approaches have been put forward refered to as correlated band theories, have been put forward in order to improve description of correlated solids. Although commonly called mean-field approaches with which they share many similarities, they are not mean-field treatments of any many-body Hamiltonian. Rather, they are approximate energy functionals based on the complete many-body Hamiltonian. Such methods are called "correlated band theory", which includes the hybrid exchange functionals (HSE), the self-interaction-corrected local spin-density method (SIC-LSD), and LSDA+Coulomb-U (LDA+U), and and each of them has had its successes in providing an improved description of some aspects of correlated solids.

In what follows, we focus on the LDA+U and its extensions as applied to the electronic, magnetic, and superconducting properties of f-electron actinide systems. Since, the actinides are heavy atoms, the relativistic effects such as spin-orbit coupling (SOC), and scalar-relativistic mass-velocity and Darwin terms have to be incorporated in quantitative correlated band theory. Simultaneous treatment of SOC together with Coulomb-U allows us to include the multiplet effects in the electronic structure calculations. This allows us to make a comparison between the theory and experimental photoemission (PE) spectra, representing an important criterion of correctness of the electronic structure calculations.

2.1 Static mean-field theory - LSDA+U

The essence of the LDA+U method is to identify atomic-like spinorbitals $\{\phi_\gamma\}$ and to treat interactions of electrons in these orbitals in a non-LDA manner. Technically, the explicit use of local orbitals and an orbitally dependent correction to the energy functional and to the LDA effective potential makes it most convenient to implement the LDA+U within a method using atomic-like orbitals as basis functions. This is true for the linearized muffin-tin orbital method (LMTO) in atomic sphere approximation (ASA), or with its full potential version, both of which are formulated in terms of atom-based orbitals, and most LDA+U work has been done with the LMTO-ASA method.

Implementation of LSDA+U in LAPW basis

The linearized augmented plane wave (LAPW) method, which makes no shape approximation and is acknowledged to be state-of-the-art in accuracy, uses a basis set of plane waves that are matched onto a linear combination of all radial solutions (and their energy dervative) inside a sphere centered on each atom. Hence the basis functions are nothing like individual atomic orbitals.

The LDA+U method is not limited to certain basis sets, but rather is more widely applicable [1] . As an example of its efficacy the implementation is applied to study the effects of strong on-site repulsion on the magnetic insulator NiO and the ferromagnetic metal Gd and

comparison with previous work on these materials is presented. It is to mention that implementation of LDA+U method in FP-LAPW basis, today is widely used in popular publically available plane-wave based computer programs (Wien2k, FLEUR, Elk and VASP).

The correlated band theory L(S)DA+U method consists of the local spin-density approximation (LSDA) augmented by a correcting energy of a multiband Hubbard type E_{ee} and a "double-counting" subtraction term E_{dc} which accounts approximately for an electron-electron interaction energy already included in LSDA. Up to date, there is no precise solution for the double counting in the conventional LDA/GGA as it does not have a diagrammatic representation that would provide explicit identification of the corresponding many-body interaction terms. Therefore, "physical" arguments prevail in the choice of V_{dc}.

Historically the first LDA+U functional is often called as an "around-mean-field" (AMF) limit of the LDA+U. In this AMF-LDA+U limit [2, 3] the interaction energy takes the form

$$E_{ee}^{\mathrm{AMF}} = \frac{1}{2} \sum_{\gamma_1,\gamma_2,\gamma_3,\gamma_4} \delta n_{\gamma_1,\gamma_2} \Big[\langle \gamma_1, \gamma_3 | V^{ee} | \gamma_2, \gamma_4 \rangle - \langle \gamma_1, \gamma_3 | V^{ee} | \gamma_4, \gamma_2 \rangle \Big] \delta n_{\gamma_3,\gamma_4} \,, \tag{1}$$

where V^{ee} is an effective on-site "Coulomb-U" interaction, the combined spin-orbital index $\gamma = (m\sigma)$ is composed from the angular m and spin index σ, and

$$\delta n_{\gamma_1,\gamma_2} = n_{\gamma_1,\gamma_2} - n^{\sigma_1} \delta_{\gamma_1,\gamma_2} \,, \quad n^{\sigma} = \frac{1}{2l+1} \sum_{m=-l}^{l} n_{m\sigma,m\sigma} \,, \tag{2}$$

where n_{γ_1,γ_2} is the on-site f-occupation matrix in the spin-orbital space which has to be defined with respect to the chosen localized orbital basis set, and n^{σ} is an average spin-orbital occupation.

In the 'fully localized" limit (FLL) [4], the double-counting term $E_{dc} == \frac{U}{2} n(n-1) - \frac{J}{2} \sum_{\sigma} n^{\sigma}(n^{\sigma}-1)$ is taken to satisfy an atomic-like limit of the LDA total energy. The LDA+U total energy functional in the FLL limit

$$E_{ee}^{\mathrm{FLL}} = \frac{1}{2} \sum_{\gamma_1,\gamma_2,\gamma_3,\gamma_4} n_{\gamma_1,\gamma_2} \Big[\langle \gamma_1, \gamma_3 | V^{ee} | \gamma_2, \gamma_4 \rangle - \langle \gamma_1, \gamma_3 | V^{ee} | \gamma_4, \gamma_2 \rangle \Big] n_{\gamma_3,\gamma_4} - E_{dc}. \tag{3}$$

We note that the essential feature of the Eq. (1) is the presence of spin-off-diagonal elements of the on-site occupation matrix $n_{\boldsymbol{\gamma_1\gamma_2}} \equiv n_{m_1\sigma_1,m_2\sigma_2}$ which are in general non-zero in the presence of the spin-orbit coupling (SOC).

The FP-LAPW method uses a basis set of plane waves that are matched onto a linear combination of all radial solutions (and their energy derivative) inside a sphere centered on each atom. In this case, we make use of the projector technique which is described in detail in Ref. [1].

Minimization of the LDA+U total energy functional leads to the set of the Kohn–Sham-like equations:

$$[-\nabla^2 + V_{\mathrm{LDA}}(\mathbf{r}) + V_U + \xi(\mathbf{l}\cdot\mathbf{s})]\Phi_{\mathbf{k}}^{b}(\mathbf{r}) = \epsilon_{\mathbf{k}}^{b} \Phi_{\mathbf{k}}^{b}(\mathbf{r}) \,, \tag{4}$$

where, the effective "LDA+U potential" , $V_U = \sum_{\gamma_1\gamma_2} |\phi_{\gamma_1}\rangle V_U^{\gamma_1\gamma_2} \langle \phi_{\gamma_2}|$, is given as,

$$V_U^{\gamma_1\gamma_2} = \sum_{\gamma\gamma'} \Big(\langle \gamma_2\gamma | V^{ee} | \gamma_1\gamma' \rangle - \langle \gamma_2\gamma | V^{ee} | \gamma'\gamma_1 \rangle \Big) n_{\gamma\gamma'} \; - \; V_{dc} \delta_{\gamma_1\gamma_2} \,. \tag{5}$$

The set of Kohn-Sham-like equations is solved self-consistently over the charge/spin densities, and occupation matrix n_{γ_1,γ_2}. It is important to mention that due to the full potential character care should be taken [5] to exclude the double-counting of the f-states non-spherical contributions to the LDA and LDA+U parts of potential in Eq. (4).

2.2 The LDA+U calculations for selected actinide materials.

Below, we illustrate the LDA+U by examples of the electronic structure calculations for selected actinide compounds. The basic difference of LDA+U calculations from the LDA/GGA is its explicit dependence on the on-site spin- and orbitally resolved occupation matrices . Minimizing the LDA+U total energy functional with SOC treated self-consistently generates not only the ground state energy and spin densities, but also effective one-electron states and energies (the band structure) that provides the orbital contribution to the moment and Fermi surfaces.

Electronic structure, magnetism and superconductivity in UGe_2

Superconductivity below 1K in the limited pressure range (1 to 1.6 GPa) was recently observed coexisting with strong ferromagnetism in a high purity single crystal UGe_2 [6] adding yet another dimension to this unanticipated phenomenon of phase coexistence. This superconducting phase is found within the ferromagnetic phase and disappears in the paramagnetic region, strongly suggesting the pairing mechanism is magnetic in origin.

We have applied the LDA+U [7, 8] to investigate the electronic structure, the magnetic character, and Fermi surfaces of the UGe_2. The magnetisation dependence on the electron pressure is shown in Fig. 1. Over a range of volumes (i.e., pressures), two nearly degenerate states FM1 and FM2, which differ most strikingly in their orbital character (on uranium), are obtained. The calculated moment (and its separation into spin and orbital parts) is consistent with the neutron scattering data. These two states are strong candidates for the two ferromagnetic phases, one low-temperature low-pressure, the other higher-temperature higher pressure. Orbital (and spin) waves built from fluctuations between these uranium configurations provide a possible different mechanism of pairing in UGe_2.

Electronic structure theory vs XMCD experiments for actinides: an example of Np_2Co_{17}

The Np_2Co_{17} is one of the few transuranium intermetallic compounds crystallizing in the hexagonal Th_2Ni_{17}-type structure. The compound orders ferromagnetically above room temperature, with a saturation magnetization M_{sat} = 30 μ_B/f.u. and a small, easy-axis magnetic anisotropy. The magnetization, Mössbauer and X-ray magnetic circular dichroism (XMCD) measurements were used to investigate the magnetic properties of Np_2Co_{17}. Analysis of he XMCD spectra yields the valence spin-orbit interaction per hole w^{110}/n_h= -0.39, μ_L = 3.55 μ_B, μ_S = -1.95 μ_B, and μ_{md} = -2.59 μ_B.

The LDA+U calculations of the newly discovered Np_2Co_{17} were performed making use of the full-potential linearized augmented plane wave (FP-LAPW) method, that includes all relativistic effects: scalar-relativistic and spin-orbit coupling (SOC). The comparison between

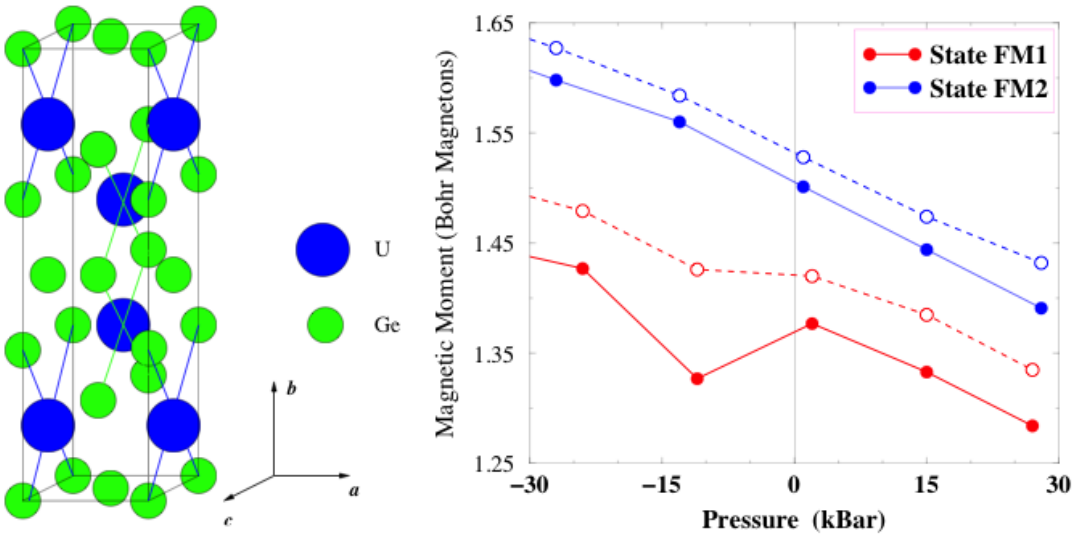

Figure 1: Pressure dependence of M_{tot} per primitive cell (full line) and M_{tot} per U-atom sphere(dashed line) for the states FM1 (lower pair of curves) and FM2 (upper pair).

Table 1: $5f$-states occupations n^{5f}, $n^{5f}_{5/2}$ and $n^{5f}_{7/2}$, branching ratio B, and $5f$-electron contribution to the valence spin-orbit interaction per hole w^{110}/n_h, and the spin, orbital, and magnetic-dipole moments (μ^{5f}_S, μ^{5f}_L, and μ_{md}) in Bohr magneton (μ_B) units.

Atom[Site]	n^{5f}	$n^{5f}_{5/2}$	$n^{5f}_{7/2}$	B	w^{110}/n_h	μ^{5f}_S	μ^{5f}_L	μ_{md}
AMF-LSDA+U								
Np[2b]	3.78	3.27	0.51	0.75	-0.38	-2.03	3.48	-2.28
Np[2d]	3.82	3.31	0.51	0.75	-0.38	-2.12	3.76	-2.44

first-principle electronic structure calculations shown in Tab. 1 and experimental data illustrates a good quantitative agreement between the LDA+U theory and experiment.

Electronic structure, magnetism and magnetic anisotropy in actinide members of "1111 family": NpFeAsO and PuFeAsO.

The first-principles electronic structure calculations for the actinide-based oxypnictides, NpFeAsO and PuFeAsO, were performed to analyze the bulk experimental data. We used the full-potential LAPW method (FP-LAPW) which includes all relativistic effects (scalar-relativistic and spin-orbit coupling), and relativistic version of the rotationally invariant LDA+U method. [9, 10] For both NpFeAsO and PuFeAsO, LDA+U yields the lowest energy anti-ferromagnetic (AF) ground state. For NpFeAsO compound, the calculated value of the total magnetic moment m_J = 2.05 μ_B (the sum of spin m_S = -2.98 μ_B, and orbital m_L = 5.03 μ_B moments) on the Np atom is found in reasonable agreement with experimental value of 1.7 μ_B for U= 3 eV. The Fe atom carries the moment μ_B = 0.11 μ_B , and there are no noticeable moments on the As and O atoms. For PuFeAsO compound, the total magnetic moment m_J = 0.41 μ_B (the m_S = -3.65 μ_B, and orbital m_L = 4.06 μ_B moments) on the Pu atom is calculated for U= 4 eV. The Fe atom has the moment m_J = 0.54 μ_B , and there are no noticeable moments on the As and O atoms.

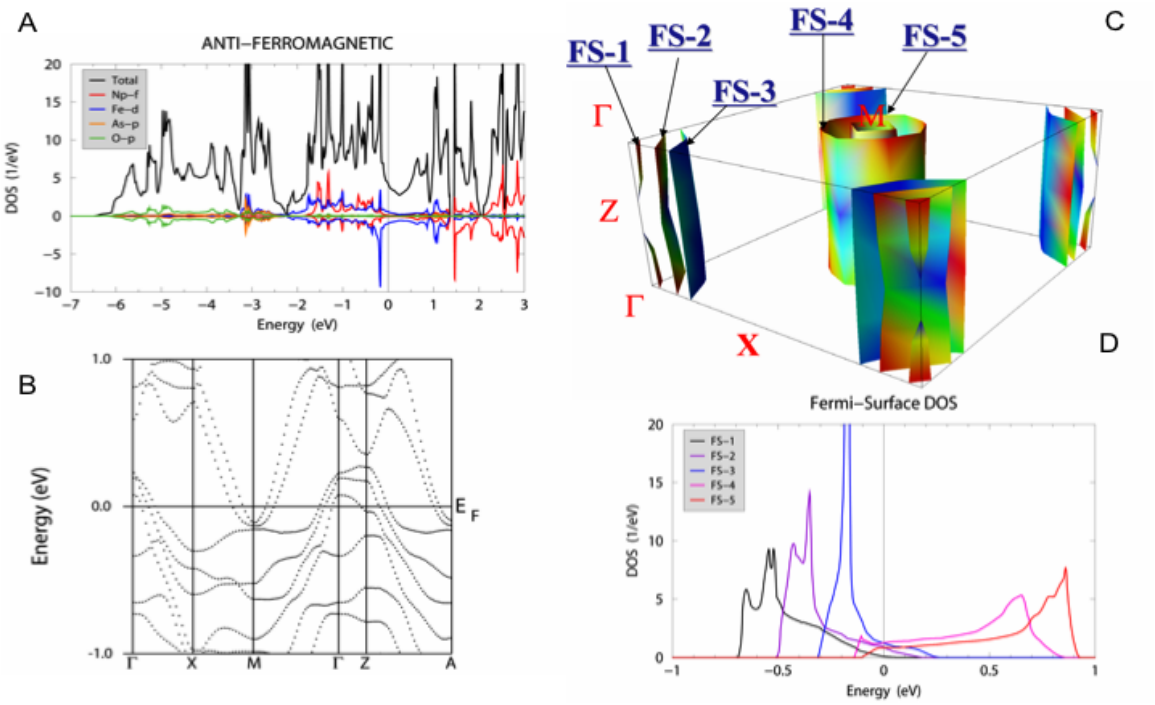

Figure 2: **Electronic structure calculations for NpFeAsO.** (a) The relativistic spin- and orbital-resolved DOS (per unit cell) including the partial DOS;(b) the band structure, and (c-d) Fermi surface for NpFeAsO, calculated making use of the FLL+LSDA+U=3 eV calculations.

The Fermi Surfaces (FS) of NpFeAsO and PuFeAsO consist of five sheets, each of them

doubly degenerate (see Fig. 2). Examination of the band structure shows that FS-1-3 sheets are hole-like, and centered at the Γ-point. The FS-4 and FS-5 are electron-like and centered at the M-A line. Note the fairly two dimensional character of the FS, and the strong resemblance to those previously presented for RFeAsO. Most of the states in the vicinity of the FS are located near Γ-[0,0,0] and M-[π,π,0] k-points in the BZ suggesting the possibility of s +/- superconducting pairing mechanism. In order to understand the absence of the orthorhombic structural distortion associated with the magnetic ordering, we performed magnetic anisotropy energy (MAE) calculations, rotating the staggered AF magnetization from the c-axis to the a-axis direction. What we found is that the total energy difference $E[a] - E[c]$ between these two directions of the magnetization is of 30.0 meV/f.u. This means that there is a strong positive uniaxial MAE in NpFeAsO. This MAE keeps the staggered AF magnetization along the tetragonal c-axis and assists in the prevention of any distortion in the a-b-plane.

2.3 Dynamical mean-field extensions of LDA+U : LDA+HIA and LDA+ED approximations.

In this section I describe the so-called local density matrix approximation (LDMA)[11, 12] to the dynamical mean-field theory, which combines the LSDA with the solution of the on-site singe impurity Anderson model. It is implemented in the full-potential linearized augmented plane wave (FP-LAPW) basis and includes full self-consistency over the charge density. The LDMA extends the LDA+U in several important aspects. It goes beyond the single Slater determinantal wave functions for the description of the intra-atomic processes and thus inherently incorporates intermediate coupling regime and accounts for multiplet transitions within the f shell.

The starting point of our approach is the multi-band Hubbard Hamiltonian [13] $H = H^0 + H^{\rm int}$. $H^0 = \sum_{i,j,\gamma} H^0_{i\gamma_1,j\gamma_2} c^\dagger_{i\gamma_1} c_{j\gamma_2}$, where i, j label lattice sites and $\gamma = (lm\sigma)$ mark spinorbitals $\{\phi_\gamma\}$, is the one-particle Hamiltonian found from *ab initio* electronic structure calculations of a periodic crystal; $H^{\rm int}$ is the on-site Coulomb interaction [13] describing the f- electron correlation. We assume that electron interactions in the s, p, and d shells are well approximated in DFT.

The effects of the interaction Hamiltonian $H^{\rm int}$ on the electronic structure are described by a **k**-independent one-particle selfenergy, $\Sigma(z)$ (where z is a (complex) energy), which is constructed with the aid of an auxiliary impurity model describing the complete seven-orbital $5f$ shell. This multi-orbital impurity model includes the full spherically symmetric Coulomb interaction, the spin-orbit coupling (SOC), and the crystal field (CF). The corresponding Hamil-

tonian can be written as [14]

$$
\begin{aligned}
H_{\mathrm{imp}} = & \sum_{\substack{kmm' \\ \sigma\sigma'}} [\epsilon^k]^{\sigma\ \sigma'}_{mm'} b^\dagger_{km\sigma} b_{km'\sigma'} + \sum_{m\sigma} \epsilon_f f^\dagger_{m\sigma} f_{m\sigma} \\
& + \sum_{mm'\sigma\sigma'} \left[\xi \mathbf{l}\cdot\mathbf{s} + \Delta_{\mathrm{CF}}\right]^{\sigma\ \sigma'}_{mm'} f^\dagger_{m\sigma} f_{m'\sigma'} \\
& + \sum_{\substack{kmm' \\ \sigma\sigma'}} \left([V^k]^{\sigma\ \sigma'}_{mm'} f^\dagger_{m\sigma} b_{km'\sigma'} + \mathrm{h.c.} \right) \\
& + \frac{1}{2} \sum_{\substack{mm'm'' \\ m'''\sigma\sigma'}} U_{mm'm''m'''} f^\dagger_{m\sigma} f^\dagger_{m'\sigma'} f_{m'''\sigma'} f_{m''\sigma},
\end{aligned}
\tag{6}
$$

where $f^\dagger_{m\sigma}$ creates an electron in the $5f$ shell and $b^\dagger_{m\sigma}$ creates an electron in the "bath" that consists of those host-band states that hybridize with the impurity $5f$ shell. The energy position ϵ_f of the impurity level, and the bath energies ϵ^k are measured from the chemical potential μ. The parameters ξ and Δ_{CF} specify the strength of the SOC and the size of the CF at the impurity. The parameter matrices V^k describe the hybridization between the $5f$ states and the bath orbitals at energy ϵ^k. The selfenergy $[\Sigma(z)]^{\sigma\ \sigma'}_{mm'}$ is then obtained from the inverse of the Green's function matrix $[G_{\mathrm{imp}}]$.

Once the selfenergy is known, the local Green's function $G(z)$ for the electrons in the solid,

$$
[G(z)]_{\gamma_1\gamma_2} = \frac{1}{V_{\mathrm{BZ}}} \int_{\mathrm{BZ}} \mathrm{d}^3k \left[z + \mu - H_{\mathrm{LDA}}(\mathbf{k}) - \Sigma(z) \right]^{-1}_{\gamma_1\gamma_2}, \tag{7}
$$

is evaluated.

LDA+Hubbard I approximation

Once the first and fourth terms are neglected, the Hamiltonian Eq.(6) is reduced to the atomic Hamiltonian H^{at}. This corresponds to the Hubbard-I approximation. Exact diagonalization diagonalization of $H^{\mathrm{at}}|\nu\rangle = E_\nu|\nu\rangle$ is performed to obtain all possible eigenvalues E_ν and eigenvectors $|\nu\rangle$.

We use the single-site approximation to solve the Eq.(7),

$$
[G(z)]^{-1}_{\gamma_1\gamma_2} = [G_{\mathrm{LDA}}(z)]^{-1}_{\gamma_1\gamma_2} - \Delta\epsilon\, \delta_{\gamma_1\gamma_2} - [\Sigma_{\mathrm{H}}(z)]_{\gamma_1\gamma_2}, \tag{8}
$$

where $\Sigma_{\mathrm{H}}(z)$ is the HIA selfenergy, $\Delta\epsilon$ accounts for the difference between the impurity and the lattice chemical potentials, and $G_{\mathrm{LDA}}(z)$ is the LDA Green's function,

$$
[G_{\mathrm{LDA}}(z)]_{\gamma_1\gamma_2} = \frac{1}{V_{\mathrm{BZ}}} \int_{\mathrm{BZ}} \mathrm{d}^3k \left[z + \mu - H_{\mathrm{LDA}}(\mathbf{k}) \right]^{-1}_{\gamma_1\gamma_2}. \tag{9}
$$

The local density matrix $n_{\gamma_1\gamma_2}$

$$
n_{\gamma_1\gamma_2} = -\frac{1}{\pi}\, \mathrm{Im} \int_{-\infty}^{E_{\mathrm{F}}} \mathrm{d}z\, [G(z)]_{\gamma_1\gamma_2}, \tag{10}
$$

is used to construct an effective LDA+U potential V_U, which is inserted into Kohn–Sham-like equations. These equations are iteratively solved until self-consistency over the charge density

is reached. The new Green function $G_{\rm LDA}(z)$ in Eq. (9) and the selfenergy $\Sigma_{\rm H}(z)$ for the new value of the f-shell occupation, obtained from the solution of Eq. (4), are evaluated. The self-consistency loop is closed by inserting the new $G_{\rm LDA}(z)$ and $\Sigma_{\rm H}(z)$ into the matrix in Eq. (8), and evaluating the new local occupation matrix $n_{\gamma_1\gamma_2}$. At the end, the imaginary part of the local Green's function $G(z)$ in Eq. (8) provides a means to estimate valence-band photoemission spectra.

LDA+"Exact diagonalization" approximation

To proceed further, we extend our procedure, and account for the hybridization between f- and non-f states in the Hamiltonian Eq.(6). In order to determine the bath parameters V^k and ϵ^k, we assume that the LDA represents the non-interacting model. We then associate the LDA Green function $G_{\rm LDA}(z)$ Eq.(9) with the Hamiltonian of Eq. (6) when the coefficients of the Coulomb interaction matrix are set to zero ($U_{mm'm''m'''} = 0$). The hybridization function $\Delta(\epsilon)$ is then estimated as $\Delta(\epsilon) = -\frac{1}{\pi}\,{\rm Im\,Tr}[G^{-1}_{\rm LDA}(\epsilon + i\delta)]$ [15]. Making use of this hybridisation function, the bath parameters V^k and ϵ_k are specified. Particular choice of those parameters for different materials will be discussed later.

The band Lanczos method [16] is employed to find the lowest-lying eigenstates of the many-body Hamiltonian $H_{\rm imp}$ and to calculate the one-particle Green's function $[G_{\rm imp}(z)]^{\sigma\ \sigma'}_{mm'}$ in the subspace of the f orbitals at low temperature. The selfenergy $[\Sigma(z)]^{\sigma\ \sigma'}_{mm'}$ is then obtained from the inverse of the Green's function matrix $[G_{\rm imp}]$.

Once the selfenergy is known, the local Green's function $G(z)$ for the electrons in the solid is calculated. The self-consistency is performed as in the case of LDA+HIA described above: with the aid of the local Green's function $G(z)$, we evaluate the occupation matrix $n_{\gamma_1\gamma_2}$, and an effective LDA+U potential V_U is constructed , which is inserted into Kohn–Sham-like equations. Subsequently, a new selfenergy $\Sigma(z)$ corresponding to the updated $5f$-shell occupation is constructed. Finally, the next iteration is started by evaluating the new local Green's function, Eq. (8) (see Fig.3 for a graphical insight).

2.4 The LDA+HIA calculations for selected actinide materials

As representative systems to illustrate the LDA+HIA numerical procedure, we select heavy actinides—Am, and Cm [11] . For all of them, the HIA is expected to provide a reasonable approximation for the selfenergy. We focus on comparison between the theory and available experimental results for valence-band photoelectron spectra (PES) as well as X-ray absorption (XAS) and electron energy-loss (EELS) spectroscopies. This comparison is often taken as important criterion of truthfulness of electronic structure calculations. Experimental valence-band PES spectra will be compared with valence spectral densities resulting from the self-consistent LDMA. For the XAS and EELS experiments, we will compare the branching ratio B as well as strength of the spin-orbit coupling w^{110} for core-to-valence $4d$–$5f$ transition [17].

The LDMA results for Am and Cm are shown in Tab. 2 in comparison with the experimental data and the results of atomic intermediate-coupling (IC) atomic calculations . The LDMA calculated $n_{5/2}$, $n_{7/2}$, branching ratio B, and spin-orbit coupling strength are close to atomic IC and experimentally derived values.

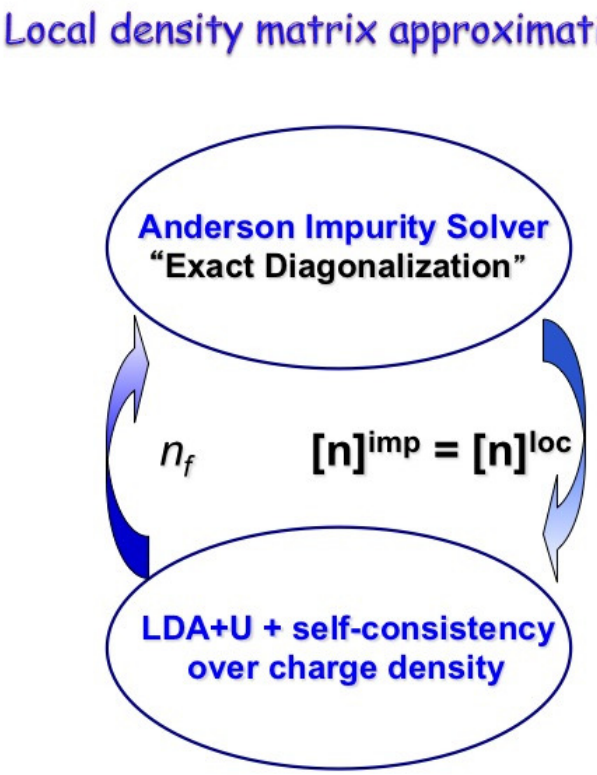

Figure 3: The self-consistent procedure for LDMA.

Am	n_f	$n_f^{5/2}$	$n_f^{7/2}$	B	w^{110}/n_h
LDMA	5.95	5.11	0.83	0.897	-0.743
atomic IC [17]	6	5.28	0.72	0.916	-0.79
Exp. [17]	6	5.38	0.62	0.930	-0.825
Cm	n_f	$n_f^{5/2}$	$n_f^{7/2}$	B	w^{110}/n_h
LDMA (β= 10 eV^{-1})	7.07	4.04	3.03	0.736	-0.340
atomic IC [17]	7	4.10	2.90	0.75	-0.37
Exp. [17]	7	4.41	2.59	0.794	-0.485

Table 2: Branching ratio B and spin-orbit coupling strength per hole w^{110}/n_h, where $n_h = (14 - n_f)$, for Am and Cm.

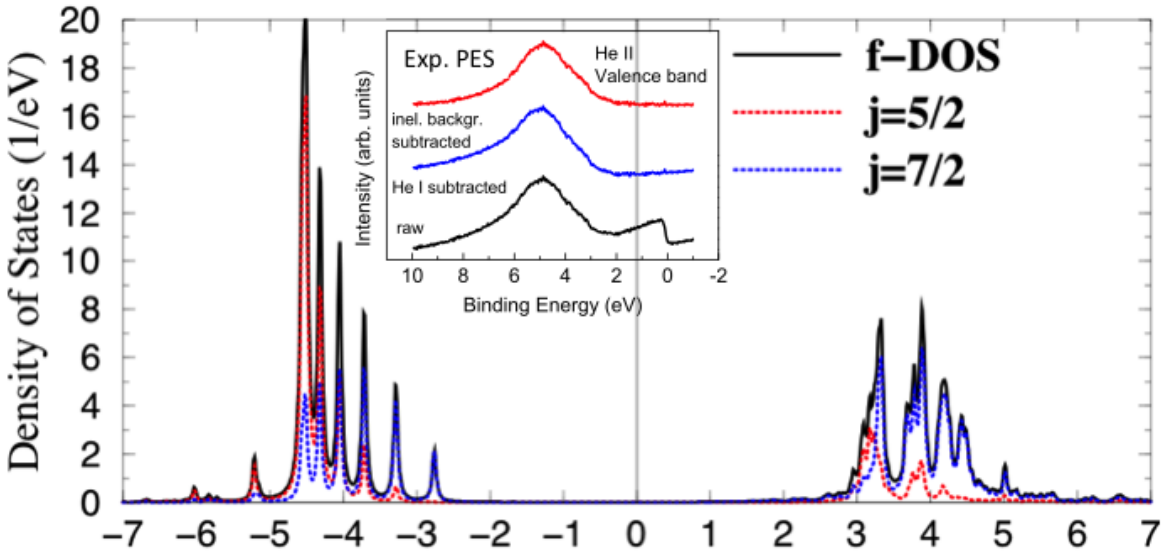

Figure 4: The Cm metal total fDOS and $j_{5/2}, j_{7/2}$ projected DOS. Insert shows the experimental PES (arb. units) from Ref. [18] is shown.

We plot in Fig. 4 total and f-projected densities of states resulting from self-consistent LDA+HIA calculations. Comparison with the experimental PES which is shown in the in the insert shows good agreement between experimental and measured PES.

3 Theory of non-magnetic ground state for δ-Pu

Plutonium exhibits six allotropic modifications at ambient pressure, some of them of very low symmetry (monoclinic). There is little doubt that this anomalous behaviour is related to the $5f$ electronic states, being at the borderline between the localized, non-bonding, behaviour and the bonding situation of electronic bands. $\delta-$Pu, residing half way between the volume of $\alpha-$Pu and Am, represents therefore generally the cross-over regime, where the electron-electron correlations play a prominent role. Katsnelson *et al.* [19] linked the broadening of the $5f$ band to the "atomic collapse" characterizing the transformation from the high-temperature expanded and the low-temperature compressed phases of Pu.

Ab-initio electron energy calculations based on the Density Functional Theory (DFT) in the Local Density (LDA) or Generalized Gradient (GGA) approximations account generally well for basic properties of metallic systems. Numerous variants of this successful paradigma were applied to Pu phases. The most conspicuous failure is the case of $\delta-$Pu calculations which inevitably lead to magnetic ordering. The fact that the lattice expansion due to magnetism yields approximately correct value of the volume, and intrasingence of magnetic order within the DFT theory both within the LDA and GGA approximations, led to speculations about magnetic ordering of $\delta-$Pu. But it contradicts experimental findings (magnetic susceptibility has a character of weak Pauli paramagnet, paramagnetic state is also evidenced ^{69}Ga NMR [20] and neutron scattering [21]).

The challenging question, which is why is there no magnetism in the δ-Pu phase, can not be answered by the DFT theory. At first, this problem is addressed making use of a well known L(S)DA+U method. Generally, the LDA+U calculations account for the on-site correlations between the f electrons in a more realistic way than the LSDA. First applied to $\delta-$Pu by Savrasov and Kotliar [4], they also lead to a magnetic solutiosav. In a contrary to [4], we apply to $\delta-$Pu a different version of the LDA+U method which is based on the original LDA+U total energy functional of Ref.[2]. We show that when the LDA+U of Ref.[2] is reformulated in a spin and orbital rotationally invariant form, it yields a basically non-magnetic $\delta-$Pu with $S_z \to 0$ and $L_z \to 0$ [22].

3.1 Magnetic moment collapse in δ-Pu: AMF-LDA+U theory

The spin M_S, orbital M_L and total M_J magnetic moments on Pu atom calculated within the LSDA (see Tab. 3) are in a very good agreement with previous LSDA calculations. The total f-state occupation $n_f = 5.06$ corresponds to $5f^5$ state. Starting from the LSDA calculated charge and spin densities and on-site spin and orbital occupations, we performed the AMF-LDA+U calculations. We choose $U = 4$ eV and exchange interaction $J = 0.7$ eV in the range of commonly accepted values for Pu [4]. Next, we turn to the salient aspect of our investigation, the AMF-LDA+U ($U = 4$ eV, $J = 0.7$ eV) calculations. Without any constraint, the calculations converged to the almost zero magnetic moment with remaining M_S and $|M_L|$ less than 0.01 μ_B. We also performed the calculations starting from a different FLL-LDA+U anti-ferromagnetic ground state and obtained essentially the same results. We conclude that the AMF-LDA+U yields fundamentally non-magnetic δ-Pu, in accordance with experimental observations. Importantly, the $5f$ occupation n_f is increased substantially from $n_f \approx 5$ in LSDA and FLL-LDA+U to $n_f = 5.44$ (see Tab. 3) meaning that there is a substantial deviation from

the $5f^5$ ionic state. We mention that the AMF-LDA+U yields $V_{eq} = 181.5$ eV and $B = 314$ kbar which are in a very good agreement with experimental data.

Table 3: Ground state spin M_S, orbital M_L, and total $M_J = M_S + M_L$ magnetic moments (in μ_B) in δ-Pu calculated for antiferromagnetic configuration at the experimental lattice parameter $a = 8.760$ a.u. using the LSDA, and AMF-LSDA+U ($U = 4$ eV) models. Also given are the equilibrium volume V_{eq} (in (a.u.)^3) and bulk modulus B.

Model	M_S	M_L	M_J	V_{eq}	B (kbar)
LSDA	4.357	-2.020	2.337	136.8	761
AMF LSDA+U	~ 0	~ 0	~ 0	181.5	314
Experiment	N/A	N/A	0	168	299

The dependence of the spin M_S, orbital M_L, and total M_J calculated within the AMF-LDA+U on the value of Coulomb-U is as follows: for small values of U ($\approx J$), δ-Pu is magnetic with sizeable M_S and M_L moments that almost cancel each other. As the U value is increased to 1.5 eV, the local moments M_S and M_L disappear and δ-Pu is non-magnetic for realistic values of the Coulomb-U (from 3 to 5 eV).

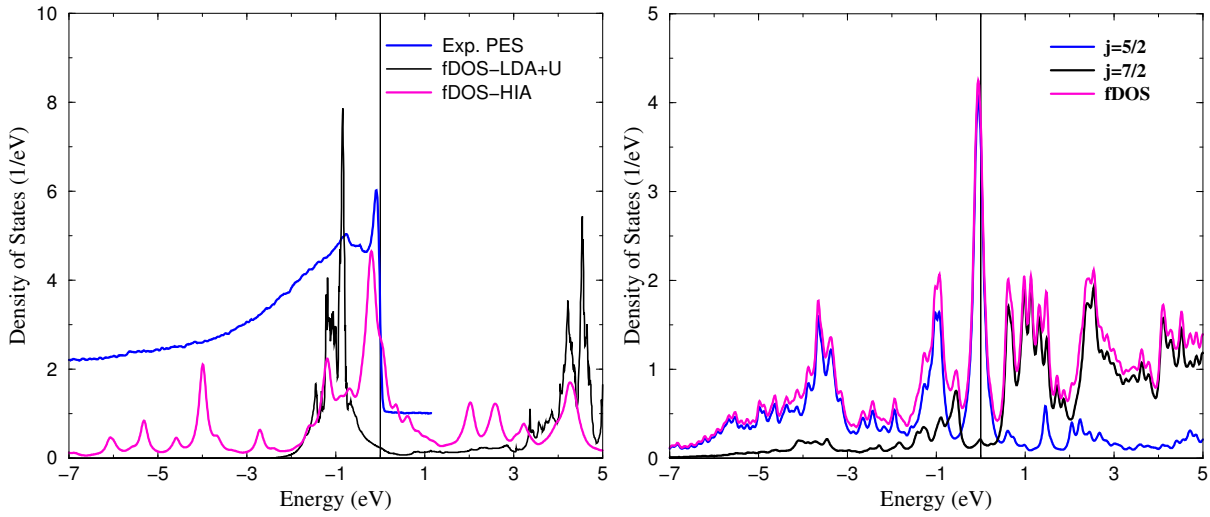

Figure 5: The δ-Pu fDOS from AMF-LDA+U and LDA+HIA calculations (a); total fDOS and $j_{5/2}, j_{7/2}$ projected DOS from LDA+ED (b). Experimental PES (arb. units) from Ref. [23] is shown.

An important criterion for assessment of results of electronic structure calculations is given by electron spectroscopies. Although some techniques, as BIS, have not been applied on Pu yet, there exists high-resolution Ultraviolet Photoelectron Spectroscopy (UPS) data, mapping the electronic structure down to about 10 eV below $E_{\rm F}$ [24, 23], while X-ray photoelectron spectroscopy [24, 23] gives information on the screening of a deep core-hole by conduction electrons.

Valence-band spectra of $\delta-$Pu and handful of other Pu-based systems studied so far exhibit invariably three narrow features, one at $E_{\rm F}$ or in its close vicinity, the other two at 0.5 and 0.85 eV below $E_{\rm F}$, which are called A, B, and C, respectively. Valence-band photoelectron

spectra reflect to some extent the density of occupied states in the ground state (DOS). A comparison with the bulk experimental UPS [24, 23] (see Fig. 5(a)) shows that LDA+U places the $5f$ manifold approximately 0.9 eV below the Fermi energy ($E_{\rm F}$) in accordance with the experimental C peak position, while it does not resolve correctly the experimental features A and B at the $E_{\rm F}$ edge.

3.2 Multiplet effects in electronic structure and photoemission of δ-Pu

In order to fix this deficiency, we extend LDA+U described above towards the DMFT to account for the multiplet transitions which are necessary for a correct description of PE excitation spectra. We use the multiorbital HIA which is suitable for incorporating the multiplet transitions in the electronic structure, as it is explicitly based on the exact diagonalization of an isolated atomic-like f-shell.

In Fig. 5(a) we show the f-projected DOS (fDOS) from AMF-LDA+U together with LDA+HIA spectral density of states. For δ-Pu, the AMF-LDA+U fDOS manifold at around -1 eV transforms into a set of multiplet transitions with high value of spectral density at E_F. There is a good agreement between the HIA calculated fDOS and the experimental PES. While LDA+HIA calculations explain well the experimental PES, the ground state of the f-shell manifold is not a singlet, this the absence of magnetism and temperature independent magnetic susceptibility remains unexplained.

To proceed further, we extend our procedure, and account for the hybridization between f- and non-f states in the Hamiltonian Eq.(6). The hybridization function $\Delta(\epsilon)$ is then estimated as $\Delta(\epsilon) = -\frac{1}{\pi}\,\mathrm{Im}\,\mathrm{Tr}[G^{-1}_{\rm LDA}(\epsilon + i\delta)]$ [15]. Also we assume that the most important hybridization is the one occurring in the vicinity of E_F, and that the hybridization matrix is, to a good approximation, diagonal in the $\{j, j_z\}$ representation, so that we only need to specify one bath state (six orbitals) with $\epsilon^{k=1}_{j=5/2}$ and $V^{k=1}_{j=5/2}$, and another bath state (eight orbitals) with $\epsilon^{k=1}_{j=7/2}$ and $V^{k=1}_{j=7/2}$. Then the bath parameters V^k_j, and the bath-state energies ϵ^k_j are chosen to approximately reproduce the LDA $5f$-states occupations $n_f^{5/2}$ and $n_f^{7/2}$.

The band Lanczos method [16] is employed to find the lowest-lying eigenstates of the many-body Hamiltonian $H_{\rm imp}$ and to calculate the one-particle Green's function $[G_{\rm imp}(z)]^{\sigma\ \sigma'}_{mm'}$ in the subspace of the f orbitals at low temperature ($k_{\rm B}T = 1/500$ eV). The selfenergy $[\Sigma(z)]^{\sigma\ \sigma'}_{mm'}$ is then obtained from the inverse of the Green's function matrix $[G_{\rm imp}]$.

In the case of δ-Pu, the hybridized ground state of the impurity is a non-magnetic singlet with all angular moments of the $5f$ plus bath cluster equal to zero ($S = L = J = 0$). It consists of $\langle n_f\rangle = 5.21$ f states and $\langle n_{bath}\rangle = 8.79$ bath states. In a pictorial way, we can imagine that the magnetic moment of the $5f$ shell (for which we get $S_f = 2.11$, $L_f = 4.21$, $J_f = 2.62$) is completely compensated by the moment carried by the electrons in the conduction band. As the value of the $5f$ magnetic moment fluctuates in time, because of the intermediate valence electronic configuration, this compensation must be understood as dynamical in nature. The $5f$-orbital projected DOS is shown in Fig. 5(b) and is in a good agreementt with the experimental PES. Notice that the multiplets for the atomic f^6 configuration ($f^6 \to f^5$ transition, lying closer to E_F) are better resolved than for the f^5 part of the spectrum ($f^5 \to f^4$ transition).

Analogously to the intermediate valence rare-earths [25], the magnetic susceptibility is anticipated to behave as $\chi \sim 1/(T + T_{fc})$, where the temperature T_{fc} describes fluctuations between

the $5f$ and conduction band electron states. T_{fc} corresponds indeed to the broadening of the quasiparticle resonance near E_F due to valence fluctuations [26]. As the ground state of the impurity is a singlet, we estimate T_{fc} using a renormalized perturbation theory of the Anderson model [14], $T_{fc} = -\frac{\pi^2}{4} Z[\Delta(E_F)/N_f]$, where $[\Delta(E_F)/N_f]$ is the hybridization per orbital at E_F, and Z is a quasi-particle weight ($Z = (\mathrm{Tr}[N(E_F)(1 - \frac{d\Sigma(\epsilon)}{d\epsilon})|_{\epsilon=E_F}]/\,\mathrm{Tr}[N(E_F)])^{-1}$. For δ-Pu we get $T_{fc} = 63$ meV ($\sim$750 K). Since T_{fc} is high, χ remains constant for $T << T_{fc}$, as observed experimentally.

4 Electronic structure of Pu-based unconventional superconductors

The intermediate-valence and non-magnetic character of the $5f$-shell can play an important role in stabilizing the superconducting state exhibited by $PuCoGa_5$ below a critical temperature T_c of 18.5 K. [27, 20, 28]. The unconventional character of superconductivity in this compound is now generally accepted but the microscopic mechanism responsible for electron pairing remains unknown. The d-wave symmetry of the superconducting gap in $PuCoGa_5$ has been proven by point contact spectroscopy experiments [29] that also provided the first spectroscopic measurements of the gap amplitude and its temperature dependence.

4.1 Electronic structure of Pu-115 family

Keeping in mind a failure of DFT in the case of δ-Pu , it can be expected that LDA/GGA does not provide a reasonable description of the electronic structure for this strongly correlated material. Below, we report electronic structure calculations of $PuCoGa_5$ performed by combining LDA with the exact diagonalization (ED) of a discretized single-impurity Anderson model, making use of the same approach as described above for δ-Pu case [30]. The calculations were carried out assuming a paramagnetic state with crystal structure parameters for $PuCoGa_5$ taken from Ref. [22]. The Slater integrals were chosen as $F_0 = 4.0$ eV, and $F_2 = 7.76$ eV, $F_4 = 5.05$ eV, and $F_6 = 3.07$ eV. They corresponds to commonly accepted values for Coulomb $U = 4.0$ eV and exchange $J = 0.64$ eV. The SOC parameter $\xi = 0.29$ eV for $PuCoGa_5$ was determined from LDA calculations. CF effects were found to be negligible and Δ_{CF} was set to zero.

The ground state of the cluster formed by the $5f$ shell and the bath is a non-magnetic singlet with all angular moments of the $5f$-bath cluster equal to zero ($S = L = J = 0$). It consists of $\langle n_f \rangle = 5.30$ f states and $\langle n_{bath} \rangle = 8.70$ bath states. The magnetic moment of the $5f$ shell (for which we get $S_f = 2.18$, $L_f = 4.05$, $J_f = 2.43$) is completely compensated by the moment carried by the electrons in the conduction band. The $5f$-orbital projected DOS is shown in Fig. 6(a). Below the Fermi energy, E_F, the DOS exhibits the three-peak structure typical for Pu and for a number of its compounds. As in case of δ-Pu, it can be noticed that the multiplets for the atomic f^6 configuration ($f^6 \rightarrow f^5$ transition, lying closer to E_F) are better resolved than for the f^5 part of the spectrum ($f^5 \rightarrow f^4$ transition).

The comparison between the DOS and experimental photoemission spectra is shown in Fig. 6(a). The three-peak structure is not resolved in the experiment which shows only the A peak at the Fermi edge. We can not claim a quantitative agreement between the DOS and the experimental PES. The shape of the total DOS corresponds fairly well to the experimental photoemission spectra. Moreover, the calculations suggest that B- and C-peaks of Pu-$5f$-states are masked by the signal coming mainly from Co-d-states. These are spread over the region from E_F to ≈ 3.5 eV.

The quasi-particle Fermi surfaces (FS) calculated using the band-structure resulting from the solutions of Eq. (4) are shown in Fig. 6(b). There are four sheets (I–IV) composing the FS: sheets I and II are fairly three-dimensional and sheets III and IV are two-dimensional. Close similarities are revealed between these sheets and the Fermi surfaces from the previous LDA [31] and AMF-LDA+U calculations.

The role of the electronic structure in determining superconductivity depends on the mechanism. First, we estimate the possibility for electron-phonon interaction mediated supercon-

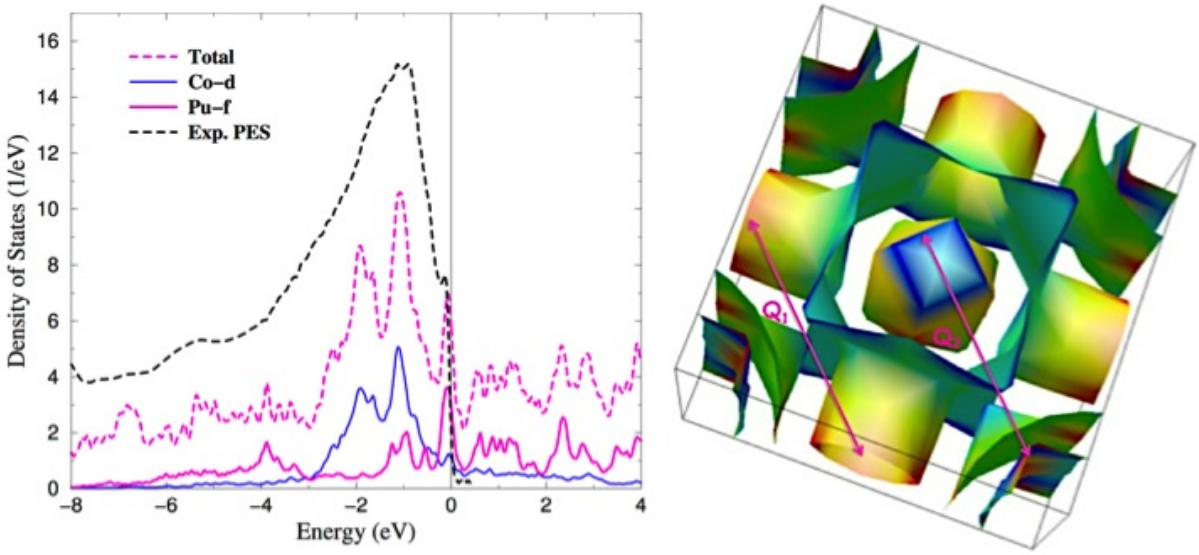

Figure 6: The $PuCoGa_5$ the total DOS, Co-dDOS, and Pu-fDOS in comparison with the experimental PES (arb. units) (a); the Fermi surface from LDA+ED (b)

ductivity. The Drude plasma energy $\Omega_p = 3.5$ eV is calculated. Now, assuming that the temperature dependence of electrical resistivity is only due to the electron-phonon interaction, we can estimate the electron-phonon coupling $\lambda_{\rm tr}$ from the Bloch–Grüneisen transport theory, employing an approximate expression[32] $\frac{\Delta\rho}{\Delta T} \approx \frac{8\pi^2}{\hbar\Omega_p^2} k_{\rm B}\lambda_{\rm tr}$ that relates the electrical resistivity ρ and the electron-phonon coupling strength. Making use of experimental room temperature ρ, we estimate the electron-phonon coupling $\lambda_{\rm tr} \approx 2.5$ for $PuCoGa_5$. Putting $\lambda_{\rm tr} = 2.5$ into the McMillan formula,[33] and assuming the Coulomb pseudopotential $\mu^* = 0.0$–0.2, we obtain an estimate for the superconducting transition temperature T_c in the range 27–39 K, which is not too far from the experimental value $T_c = 18.5$ K. This observation would supports the strong electron-phonon coupling mechanism of superconductivity in $PuCoGa_5$. However, recent point-contact spectroscopy measurements [29] are pointing on d-wave symmetry of the superconducting gap, making the electron-phonon coupling mediated superconductivity unlikely.

It has been argued that in some cases, superconductivity can be driven by Fermi surface nesting. Nesting, which indicates instability in the FS, can give rise to a spin density wave or charge density wave. The shape of FS shown in Fig. 3 suggests a possibility of either Q_1-nesting between [π,0,k_z] and equivalent k-points of FS-II sheet or Q_2-nesting between the hole-like FS-1 around the $\Gamma = (0, 0, k_z)$ point and electron-like FS-3 around the $M = (\pi, \pi, k_z)$ point. This $q \sim (\pi, \pi, k_z)$ nesting-like feature can lead to a peak in the spin/charge susceptibility, and

promote the anti-ferromagnetic or charge fluctuations to develop. The Q_1 nesting instability will promote the $d_{x^2-y^2}$ type of pairing. Recent point-contact spectroscopy measurements [29] are pointing on d-wave scenario.

The Q_2 nesting would correspond to so-called $s\pm$ superconductivity [34] similar to Fe-based superconductors [35]. The strength of the pairing interaction depends on the joint density of states. For the Q_2 nesting, it would mean a high value of the product of the DOS near $\Gamma = (0, 0, k_z)$ and $M = (\pi, \pi, k_z)$ points. As follows from the band structure, it is not the case for $PuCoGa_5$. On the other hand, possibility of the Q_1 nesting instability, together with experimental data of [29] support the d-wave scenario. The presence of a $5f$ local moment dynamically compensated by the surrounding conduction electrons, together with the f^5-f^6 intermediate-valence ground state in $PuCoGa_5$, opens an attractive possibility for valence fluctuations mediated superconductivity, similarly to heavy-fermion superconductors [36].

4.2 Unified character of correlation effects in δ-Pu and Pu-based superconductors

We have shown [30] that the the unusual physical properties of the Pu-115 compounds and of delta-Pu, in particular the unexpected absence of magnetism, may have a common origin in the intermediate-valence nature of the Pu 5f-electron ground state. In all three compounds the Pu atoms exhibit a $5f^5$-$5f^6$ intermediate-valence ground state, with a partial delocalization of the $5f^5$ multiplet. The Pu f-shell carries a non-vanishing average moment as it fluctuates between the singlet and the sextet. In the same time, the ground state of the entire impurity model is a singlet that corresponds to all angular momenta being equal to zero. Thus, the magnetic fluctuations in the f-shell are accompanied by canceling antiferromagnetic fluctuations in the conduction bands, resulting in temperature-independent magnetic susceptibility at low temperatures. The local 5f magnetic moment is compensated by a moment in the surrounding cloud of conduction electrons. In the case of $PuCoGa_5$ and δ-Pu the compensation is complete and the Anderson impurity grounds state is a non-magnetic singlet. Our findings can be important for understanding the superconductivity in these materials.

5 Conclusions

To summarise, the correlated band theory methods, both static LDA+U and dynamical LDA+HIA and LDA+ED are formulated and implemented in the FP-LAPW basis. The rotationally invariant full Coulomb vertex together with spin-orbit coupling are included in the calculations. The given examples shown that correlated band theory is capable to account correctly for the orbital polarization which helps to explain anisotropic magnetic properties in selected f-electron materials.

The material specific theory of δ-Pu is presented. Tt is shown that AMF-LDA+U is capable to explain the non-magnetic character of δ-Pu ground state. Further application of LDA+HIA and LDA+ED allows to incorporate the multiplet transitions into the electronic structure calculations, and to explain the experimental photoemission spectroscopy data. The agreement between the theory and photoemission spectra is often taken as a confirmation of the validity of the theory.

The electron correlation effects in the electronic structure of $PuCoGa_5$ and related the Pu-115 family of unconventional superconductors are considered. It is shown that the singlet ground state can form in PuCoGa5 similar to δ-Pu, with the local 5f magnetic moment is compensated by a moment in the surrounding cloud of conduction electrons. This explains the temperature independent susceptibility and non-magnetic character of these materials. At the same time, it supports the unconventional, most likely d-wave mechanism of superconductority in these materials. Our findings are important for the theory of the unconventional superconductivity in the Pu-115 family. They can assist in finding the nature of a pairing boson.

Bibliography

[1] A. B. Shick, A. I. Liechtenstein, and W. E. Pickett, Phys. Rev. B **60**, 10763 (1999).

[2] V. Anisimov, Z. J., and O. Andersen, Phys. Rev. B **44**, 943 (1991).

[3] M. Czyzyk and G. A. Sawatzky, Phys. Rev. B **49**, 14211 (1994).

[4] S. Savrasov and G. Kotliar, Phys. Rev. Lett **84**, 3670 (2000).

[5] A. B. Shick, V. Janis, V. Drchal, and W. E. Pickett, Phys. Rev. B **70**, 134506 (2004).

[6] S. Saxena *et al.*, Nature **406**, 587 (2000).

[7] A. B. Shick and W. Pickett, Phys. Rev. Lett. **86**, 300 (2001).

[8] A. Shick, V. Janis, V. Drchal, and W. E. Pickett, Phys Rev. B **70**, 134506 (2004).

[9] T. Klimczuk, H. C. Walker, R. Springell, A. B. Shick, A. H. Hill, P. Gaczyński, K. Gofryk, S. A. J. Kimber, C. Ritter, E. Colineau, et al., Phys. Rev. B **85**, 174506 (2012).

[10] T. Klimczuk, A. B. Shick, H. Springell, C. Walker, A. H. Hill, E. Colineau, J.-C. Griveau, D. Bouexiere, R. Eloirdi, and C. R., Phys Rev. B **87**, 174510 (2012).

[11] A. B. Shick, J. Kolorenc, A. I. Lichtenstein, and L. Havela, Phys. Rev. B **80**, 085106 (2009).

[12] A. B. Shick, J. Rusz, J. Kolorenc, P. M. Oppeneer, and L. Havela, Phys. Rev. B **83**, 155105 (2011).

[13] A. I. Lichtenstein and M. I. Katsnelson, Phys. Rev. B **57**, 6884 (1998).

[14] A. Hewson, *The Kondo Problem to Heavy Fermions* (Cambridge University Press, 1993).

[15] O. Gunnarsson, O. K. Andersen, O. Jepsen, and J. Zaanen, Phys. Rev. B **39**, 1708 (1989).

[16] J. Kolorenc, A. Poteryaev, and A. I. Lichtenstein, Phys. Rev. B **85**, 235136 (2012).

[17] K. Moore and G. van der Laan, Rev. Mod. Phys. **81**, 235 (2009).

[18] T. Gouder *et al.*, Phys Rev. B **83**, 123111 (2011).

[19] M. I. Katsnelson, I. V. Solovyev, and A. V. Trefilov, JETP Letters **56**, 276 (1992).

[20] N. J. Curro *et al.*, Nature **434**, 622625 (2005).

[21] J. C. Lashley, A. Lawson, R. J. McQueeney, and G. H. Lander, Phys. Rev. B **72**, 054416 (2005).

[22] A. Shick, V. Drchal, and L. Havela, EPL **69**, 588 (2005).

[23] L. Havela, T. Gouder, and F. Wastin *et al.*, Phys. Rev. B **65**, 235118 (2002).

[24] T. Gouder and et al., Europhys. Lett. **55**, 705 (2001).

[25] D. Khomskii, Soviet Physics - Uspekhi **129**, 443 (1979).

[26] C. M. Varma and Y. Yafet, Phys. Rev. B **13**, 2950 (1976).

[27] J. Sarrao *et al.*, Nature **420**, 297 (2002).

[28] F. Jutier *et al.*, Phys. Rev. B **77**, 024521 (2008).

[29] D. Daghero and et al., Nature Communications **3**, 1785 (2012).

[30] A. B. Shick, J. Rusz, J. Kolorenc, P. M. Oppeneer, A. I. Lichtenstein, M. I. Katsnelson, and R. Caciuffo, Phys. Rev. B **87**, 020505 (2011).

[31] A. Shick, V. Janis, and P. Oppeneer, Phys. Rev. Lett **94**, 016401 (2005).

[32] P. B. Allen, Phys. Rev. B **36**, 2920 (1987).

[33] W. L. McMillan, Phys. Rev. **167**, 331 (1968).

[34] T. Das, J.-X. Zhu, and M. Graf, arXiv:13111610 (2013).

[35] I. I. Mazin, D. J. Singh, and M. D. Johannes *et al.*, Phys. Rev. Lett **101**, 057003 (2008).

[36] K. Miyake, J. Phys. Condens. Matter **19**, 125201 (2007).

List of papers

This thesis is based on the following papers (below they are listed in a chronological order) which are reffered to in the text by their Roman numerals:

I. A.B. Shick, A.I. Liechtenstein, W.E. Pickett, **"Implementation of the LDA+U method using the full potential linearized augmented plane wave basis"**, Phys. Rev. B **60**, 10763 (1999).
II. A.B. Shick, W.E. Pickett, C.S. Fadley, **"Electron correlation effects and magnetic ordering at the Gd(0001) surface"** , Phys. Rev. B **61** - Rapid Comm., 9213 (2000).
III. A. B. Shick and W. E. Pickett, **"Magnetism, Spin-Orbit Coupling and Superconducting Pairing in UGe_2**, Phys. Rev. Lett. **86**, 300 (2001).
IV. A. B. Shick, V. Janiš, V. Drchal, and Warren E. Pickett, **"Spin and Orbital Magnetic State of UGe2 under Pressure"**, Phys. Rev. B **70**, 134506 (2004).
V. A. B. Shick, V. Janiš, and P. M. Oppeneer, **"Effect of Coulomb correlations on the electronic structure of $PuCoGa_5$"**, Phys. Rev. Lett. **94** , 016401 (2005).
VI. A. B. Shick, V. Drchal, and L. Havela, **"Coulomb- U and magnetic-moment collapse in δ- Pu"**, Europhys. Lett. **69** , 588 (2005).
VII. A. B. Shick, L. Havela, J. Kolorenc, V. Drchal, Thomas Gouder, and Peter M. Oppeneer, **"Electronic structure and nonmagnetic character of δ-Pu-Am alloys"**, Phys. Rev. B **73** , 104415 (2006).
VIII. A. B. Shick, J. Kolorenc, A.I. Lichtenstein, L. Havela, **"Electronic structure and spectral properties of Am, Cm, and Bk: Charge-density self-consistent LDA plus HIA calculations in the FP-LAPW basis"**, Phys. Rev. B **80** , 085106 (2009).
IX. T.Gouder, G. van der Laan, A. B. Shick, R. G. Haire, and R. Caciuffo, **"Electronic structure of elemental curium studied by photoemission"**, Phys. Rev. **B 83**, 125111 (2011).
X. A. B. Shick, J. Rusz, J. Kolorenc, P. M. Oppeneer, and L. Havela, **"Theoretical investigation of electronic structure, electric field gradients, and photoemission of PuCoGa5 and PuRhGa5 superconductors"**, Phys. Rev. **B 83**, 155105 (2011)
XI. I. Halevy, A. Hen, I. Orion, E. Colineau, R. Eloirdi, J.-C. Griveau, P. Gaczynski, F. Wilhelm, A. Rogalev, J.-P. Sanchez, M. L. Winterrose, N. Magnani, A. B. Shick, and R. Caciuffo, **"Structural, electronic, and magnetic characteristics of Np_2Co_{17}"**, Phys. Rev. **B 85**, 014434 (2012)
XII. D. Daghero , M. Tortello, G.A. Ummarino, J.-C. Griveau, E. Colineau, R. Eloirdi , A.B. Shick , J. Kolorenc , A. I. Lichtenstein, and R. Caciuffo, **"Strong-coupling d -wave superconductivity in $PuCoGa_5$ probed by point-contact spectroscopy"**, Nature Communications **3**, 786 (2012). (2012).
XIII. T. Klimczuk, H. C. Walker, R. Springell, A. B. Shick, A. H. Hill, P. Gaczynski, K. Gofryk, S. A. J. Kimber, C. Ritter, E. Colineau, J.-C. Griveau, D. Bouexi'ere, R. Eloirdi, R. J. Cava, and R. Caciuffo, **"Negative thermal expansion and the absence of a structural transition in NpFeAsO"**, Phys. Rev. **B 85**, 174506 (2012).
XIV. T. Klimczuk, A. B. Shick, R. Springell, H. C. Walker, A. H. Hill, E. Colineau, J.-C. Griveau, D. Bouexiere, R. Eloirdi, R. Caciuffo,**"Bulk properties and electronic structure of PuFeAsO"**, Phys. Rev. **B 86**, 174510 (2012).
XV. A. B. Shick, J. Kolorenc, J. Rusz, P. M. Oppeneer, A. I. Lichtenstein, M. I. Katsnelson, and R. Caciuffo, **"Unified character of correlation effects in unconventional Pu-based superconductors and δ-Pu"**, Phys. Rev. **B 87**, 020505(R) (2013).

Resume

This dissertation is the commented collection of 15 of my papers published in the period from 1999 to 2013 in a field of electronic structure of actinides. The correlated band theory methods, both static LDA+U and dynamical LDA+HIA and LDA+ED are formulated and implemented in the FP-LAPW basis. The theory is applied to the investigation of a number of complex actinide materials. Given examples shown that correlated band theory is capable to account correctly for the orbital polarization which helps to explain anisotropic magnetic properties in selected f-electron materials.

The material specific theory of δ-Pu is presented. It is shown that AMF-LDA+U is capable to explain the non-magnetic character of δ-Pu ground state. Further application of LDA+HIA and LDA+ED allows to incorporate the multiplet transitions into the electronic structure calculations, and to explain the experimental photoemission spectroscopy data. The agreement between the theory and photoemission spectra can serve as a confirmation of the validity of the theory.

The electron correlation effects in the electronic structure of $PuCoGa_5$ and related the Pu-115 family of unconventional superconductors are considered. The temperature independent susceptibility and non-magnetic character of these materials are explained. It is shown that the singlet ground state can form in PuCoGa5 similar to δ-Pu, with the local 5f magnetic moment is compensated by a moment in the surrounding cloud of conduction electrons. At the same time, it supports the unconventional, most likely d-wave mechanism of superconductority in these materials. Our findings are important for the theory of the unconventional superconductivity in the Pu-115 family. They can assist in finding the nature of a pairing boson.